Research in Astronomy and Astrophysics, 24:125007 (8pp), 2024 December https://doi.org/10.1088/1674-4527/ad90b0

Latitudinal and Solar Cycle Distribution of Extreme (⩾X5) Flares During 1976–2018

Qi Li[1], Xi-Wen Zhang[1], and Gui-Ming Le[2,3]
[1] Institute of Geophysics, China Earthquake Administration, Beijing 100081, China
[2] Key Laboratory of Space Weather, National Satellite Meteorological Center (National Center for Space Weather), China Meteorological Administration, Beijing 100081, China; Legm@cma.gov.cn
[3] Innovation Center for FengYun Meteorological Satellite (FYSIC), Beijing 100081, China
Received 2024 September 23; revised 2024 November 07; accepted 2024 November 08; published 2024 December 2

Abstract

We studied the latitudinal and solar cycle distribution of extreme (⩾X5) solar flares spanning 1976–2018. We found that all such flares were confined within the latitudinal range of [S30, N35]. Nonetheless, the majority of these flares during different solar cycles were confined in different latitudinal scopes. Statistical results showed that the southeast quadrant experienced the highest activity of extreme flares. 47.5% of the extreme flares occurred within the latitudes ⩽15° of the two hemispheres, with 26.2%, 31.1%, and 42.6% in the latitudinal bands [5°, 10°], >20° and [11°, 20°] of both hemispheres, respectively. Significant N–S asymmetries were observed in the ascending phase of SC 21, the descending phase of SC 23, and both phases of SC 24. Other phases showed asymmetries primarily in latitudinal distribution. The proportion of extreme flares in the ascending phases of SCs 21–24 was 22.2%, 33.3%, 38.9%, and 50%, respectively. Stronger flares (⩾X10) were more likely to occur in the descending phase, with 39% of X5–X9 flares and 20% of (⩾X10) flares occurring in the ascending phase. On average, 83.6% of extreme flares occurred within a period extending from two years prior to three years following the solar peak, according to our statistical analysis, with specific percentages for each cycle being 88.9%, 100%, 61.1%, and 75%.

Key words: Sun: flares – (Sun:) sunspots – Sun: X-rays – gamma-rays

1. Introduction

A solar flare is defined as a sudden, rapid, and intense variation in brightness. Flares are usually produced by sunspots, which are also termed active regions (ARs). Solar flares usually emit intense bursts of electromagnetic radiation. The peak flux in 1–8 nm wavelength band during a solar flare is defined as the intensity of a solar soft X-ray flare. For the convenience of description, solar soft X-ray flare is termed as solar flare or flare in this study. The largest class flares are X-class flares. The smallest class flares are A-class flares, followed by B, C, M and X-class flares. A solar cycle usually produces a huge number of solar flares. A and B-class flares are very weak flares and have little influence on space weather. Hence, we do not pay attention to A and B-class flares. It was found that the number of ⩾C1.0 is 37 851 with the proportion of X-class flares lower than 1% (Veronig et al. 2002). The fraction of X-class flares is less than 1% of ⩾C1.0 flares during cycles 2123 (Joshi et al. 2010). These statistical results indicate that X-class flares are very strong flares and termed as great flares (Verma 2011). It was found that ⩾X5 flares accounted for about 13% of the X-class flares during solar cycles 21–23 (Le et al. 2014), indicating that ⩾X5 flares are very rare. ⩾X5 flares are termed extreme solar flares in this study. An AR that can produce very strong eruptions is termed as super active region (SAR). Different researchers have different definitions of SARs (e.g., Bai 1987; Bai 1988; Roy 1997; Tian et al. 2002; Romano & Zuccarello 2007; Chen et al. 2011 and references therein). It was found that 83.9% of the extreme flares were produced by SARs (Le et al. 2021a). Statistical studies showed that the 11°–20° latitude belt of both hemispheres of the Sun produced the most flares (e.g., Joshi et al. 2010; Pandey et al. 2015; Joshi & Chandra 2019). Are these statistical results correct for the extreme flares? Chapman & Dudok de Wit (2024) found that the most extreme space weather events occur when >90% of solar active region areas have moved to within about 15° of the solar equator. Is this conclusion correct for the extreme flares?

The distribution of extreme flares across solar cycles provides insights into the timing of their occurrence within each cycle. Numerous studies have focused on the solar cycle distribution of various extreme space weather events (e.g., Kilpua et al. 2015; Hajra et al. 2016; Lefèvre et al. 2016; Vennerstrom et al. 2016; Meng et al. 2019; Le & Liu 2020, Le et al. 2021b, 2021c, 2021d; Owens et al. 2021; Chapman et al. 2020; Chapman & Dudok de Wit 2024). Lin et al. (2023) investigated the evolution of solar soft X-ray flares of varying

intensities in relation to the solar cycle and their association with sunspot groups. However, the latitudinal and solar cycle distribution of extreme flares from 1976 to 2018 remains unexplored. The current inquiry seeks to uncover the patterns of extreme flares during the ascending and descending phases of the solar cycle from 1976 to 2018 and to determine the number of extreme flares that occurred around the period of solar maximum.

Smoothed Monthly Mean Sunspot Numbers (SMMSNs), which were reconstructed and released in 2015 July by Clette et al. (2014) and Clette & Lefèvre (2016), are extensively utilized to track the progression of solar cycles. The latitudinal and solar cycle distribution of extreme flares constitutes crucial information that could potentially validate solar dynamo theories. Therefore, examining the latitudinal and solar cycle distribution of extreme flares is of significant interest. This study aims to address the question: What patterns emerged in the latitudinal and solar cycle distribution of extreme flares between 1976 and 2018? The remainder of this paper is structured as follows: Section 2 presents the data analysis, Section 3 discusses the findings, and the final section draws conclusions.

2. Data Analysis

2.1. Data Source

The data on extreme solar flares were sourced from the NOAA's National Geophysical Data Center, accessible via the FTP link: ftp://ftp.ngdc.noaa.gov/STP/space-weather/solar-data/solar-features/solar-flares/x-rays/goes/xrs/. For the smoothed monthly mean sunspot numbers, the data were retrieved from the Royal Observatory of Belgium's Solar Influences Data Analysis Center, which can be accessed at https://www.sidc.be/SILSO/datafiles.

2.2. Latitudinal Distribution of the Extreme Flares

The latitudinal distribution of extreme flares from 1976 to 2018 is presented in the Appendix. Based on the temporal data and latitudes of the extreme flares listed in the Appendix, along with the SMMSNs, Figure 1 illustrates the latitude distribution of extreme flares during the ascending and descending phases of Solar Cycles 21 and 22. The designations SC 21A and SC 21D refer to the ascending and descending phases of Solar Cycle 21, respectively, while SC 22A and SC 22D denote the ascending and descending phases of Solar Cycle 22. Additionally, NHLS and SHLS are used to indicate the latitudinal ranges of extreme flares in the northern and southern hemispheres, respectively.

The source locations of extreme flares occurring during the ascending phase of Solar Cycle 21 are depicted in the upper left panel of Figure 1. During this phase, extreme flares were exclusively found in the northern hemisphere within the latitudinal range of [N05, N22]. The upper right panel of Figure 1 displays the source locations of extreme flares in the descending phase of Solar Cycle 21. In this phase, there were five extreme flares in the northern hemisphere and nine in the southern hemisphere. The northern hemisphere flares were distributed between latitudes [N11, N24], while those in the southern hemisphere spanned from [S08, S12]. Out of the total 18 extreme flares, 16 were concentrated within the latitudinal belt of 5°–18° in both hemispheres.

The left lower panel of Figure 1 illustrates the extreme flares during the ascending phase of Solar Cycle 22, which numbered seven in total. Three of these flares originated in the northern hemisphere, with latitudes at N30, N33, and N35, respectively. The remaining four flares were from the southern hemisphere and were distributed within the latitudinal range of [S20, S30]. The right lower panel of Figure 1 displays the source locations of 15 extreme flares during the descending phase of Solar Cycle 22, with eight occurring in the northern hemisphere and six in the southern hemisphere. Within the northern hemisphere, seven of these flares were concentrated between latitudes [N25, N34], while the six southern hemisphere flares spanned the range [S13, S26]. This distribution suggests an asymmetric pattern in the latitudinal occurrence of extreme flares between the northern and southern hemispheres. Across Solar Cycle 22, a total of 21 extreme flares were recorded, with 18 of them falling within the latitudinal belt of 20° to 35° in both hemispheres. A detailed latitudinal distribution of the extreme flares for both the ascending and descending phases of Solar Cycles 21 and 22 is presented in Table 1.

We denote the ascending and descending phases of Solar Cycle 23 as SC 23A and SC 23D, respectively, and those of Solar Cycle 24 as SC 24A and SC 24D, respectively. Figure 2 presents the latitudinal distribution of extreme flares during the ascending and descending phases of Solar Cycles 23 and 24, based on their source locations and SMMSNs. In the ascending phase of Solar Cycle 23, depicted in the upper left panel of Figure 2, there were seven extreme flares: three in the northern hemisphere within the latitudinal range of [N16, N22], and four in the southern hemisphere within the range of [S17, S21]. During the descending phase of Solar Cycle 23, there were 11 extreme flares; one in the northern hemisphere and ten in the southern hemisphere, with the southern flares distributed across the latitudinal range of [S05, S21]. The ascending phase of Solar Cycle 24, as shown in the lower left panel of Figure 2, had only two extreme flares, both at the same latitude of N17. Similarly, the descending phase of Solar Cycle 24, shown in the lower right panel of Figure 2, also featured two extreme flares, both in the southern hemisphere at the same latitude of S08. A detailed latitudinal distribution of the extreme flares during the ascending and descending phases of Solar Cycles 23 and 24 is tabulated in Table 2.

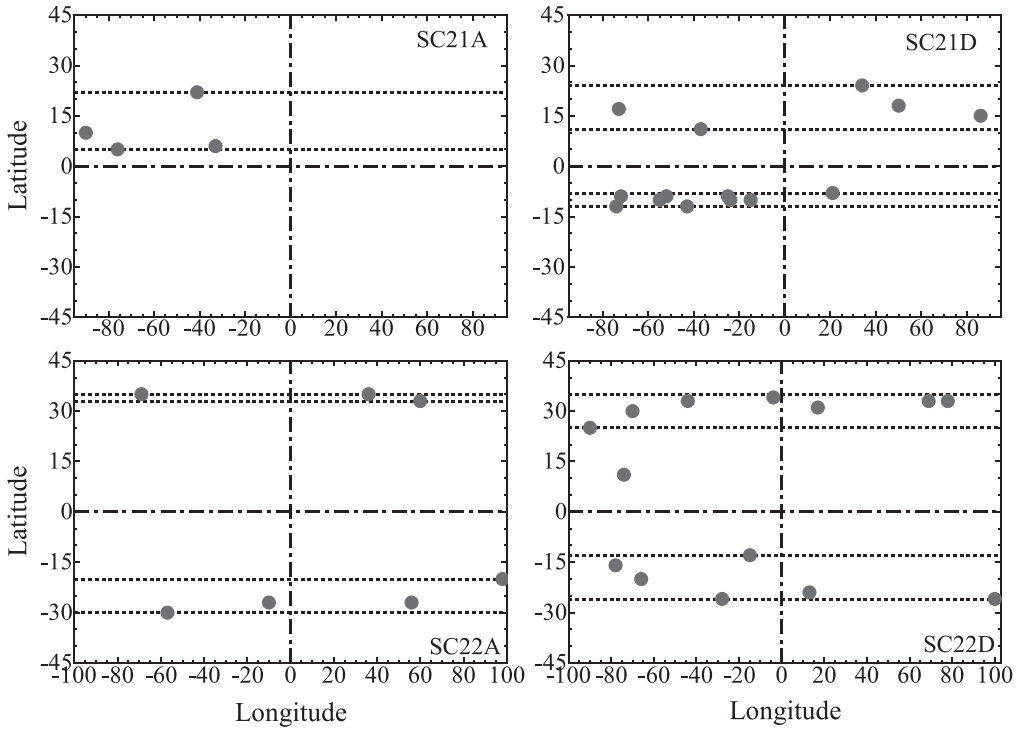

Figure 1. The source locations of the extreme flares during ascending and descending phases of solar cycles 21 and 22. The left and right upper panels denote the source locations of the extreme flares in the ascending and descending phases of solar cycle 21, respectively. The left and right lower panels denote the source locations of the extreme flares in the ascending and descending phases of solar cycle 22, respectively.

Table 1
Latitudinal Distribution of the Extreme Flares During SCs 21 and 22

Period	SC 21A	SC 21D	SC 22A	SC 22D
NHLS	[N05, N22]	[N11, N24]	N30, N33, N35	[N11, N34]
NHLS	Null	[S08, S12]	[S20, S30]	[S13, S26]

2.3. Solar Cycle Distribution of the Extreme Flares

Using the time of the sunspot maximum as the reference point (time 0.0) and normalizing the times of the two adjacent sunspot minima to −1.0 and 1.0, respectively, some researchers (e.g., Kilpua et al. 2015; Meng et al. 2019) define the period between −0.2 and 0.2 as the solar maximum. Consequently, a solar cycle is divided into four distinct periods: solar minimum, ascending phase, solar maximum, and descending phase. However, we define the ascending phase of a solar cycle as the period from the first month of the cycle to the month when the SMMSNs reach their peak value. The descending phase is defined as the period from the first month after the SMMSNs peak to the last month of the solar cycle. Additionally, we focus on the proportion of extreme flares that occur during the period from two years before to three years after the peak of a solar cycle.

Based on the temporal data and the source locations of extreme flares detailed in the Appendix, along with the SMMSNs, Figure 3 displays the solar cycle distribution of extreme flares from 1976 to 2018. We denote the number of extreme flares occurring during the ascending phase, descending phase, and the period from two years before to three years after a solar cycle peak as N_a, N_d, and N_{23}, respectively. Additionally, N_t represents the total number of extreme flares per solar cycle. The derived ratios of N_a/N_t for Solar Cycles 21–24 were 22.2%, 33.3%, 38.9%, and 50%, respectively, suggesting that the lower the amplitude of a solar cycle, the higher the proportion of extreme flares occurring in its ascending phase. The ratios of N_d to N_t for these cycles were 77.8%, 66.7%, 61.1%, and 50%, respectively, indicating that the weaker a solar cycle, the lower the proportion of extreme flares in its descending phase. The ratios of N_{23} to N_t for Solar Cycles 21–24 were 88.9%, 100%, 61.1%, and 75%, respectively, which implies that the proportion of extreme flares occurring around the solar maximum does not appear to be directly related to the amplitude of the solar cycle. The statistical average of N_{23} to N_t across Solar Cycles 21–24 is 83.6%, indicating that, in general, the majority of extreme flares tend to occur around the time of solar maximum.

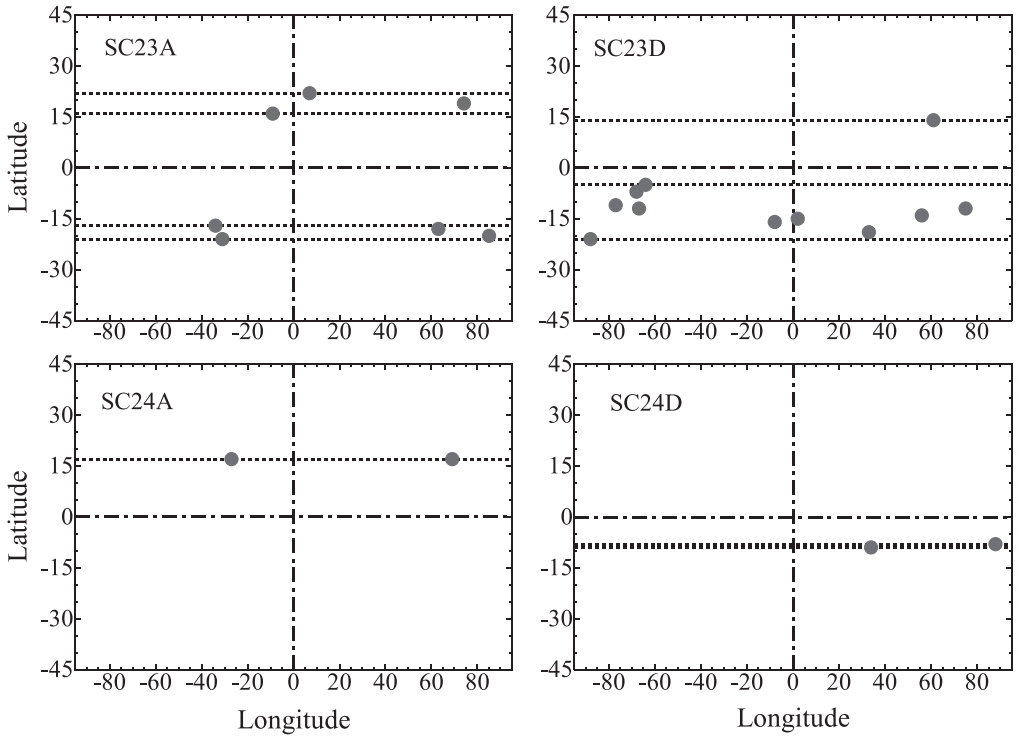

Figure 2. The source locations of the extreme flares during ascending and descending phases of solar cycles 23 and 24. The left and right upper panels denote the source locations of the extreme flares in the ascending and descending phases of solar cycle 23, respectively. The left and right lower panels denote the source locations of the extreme flares in the ascending and descending phases of solar cycle 24, respectively.

Table 2
Latitudinal Distribution of the Extreme Flares During SCs 23 and 24

Period	SC 23A	SC 23D	SC 24A	SC 24D
NHLS	[N16, N22]	N14	N17, N17	Null
SHLS	[S17, S21]	[S05, S21]	Null	S08, S08

3. Discussion

Sunspots typically emerge in the high-latitude regions of both solar hemispheres at the onset of a solar cycle and then progressively migrate toward lower latitudes, eventually disappearing in the low-latitude regions near the equator, as observed by Maunder (1922). Analyzing the latitudinal distribution of soft X-ray flares across Solar Cycles 21–23, researchers such as Joshi et al. (2010), Pandey et al. (2015), and Joshi & Chandra (2019) discovered that the 1120° latitude belt in both hemispheres was the most prolific in producing flares. However, during the ascending phase of Solar Cycle 22, extreme flares in the northern hemisphere were notably concentrated between N33 and N35, while those in the southern hemisphere were largely confined to the range of S20–S30. In the descending phase of Solar Cycle 22, 14 extreme flares occurred, with 10 of them distributed at latitudes above 20° in both hemispheres. This suggests that the generalization regarding the 1120° latitude belt as the most flare-active may not hold true for the extreme flares observed during Solar Cycle 22. Chapman & Dudok de Wit (2024) posited that the majority of extreme space weather events occur when over 90% of solar active regions are within approximately 15° of the solar equator. However, this conclusion does not align with the distribution of extreme flares during Solar Cycle 22, or the ascending phases of Solar Cycles 23 and 24.

Statistical distribution of the source locations of the all extreme flares during 1976–2018 was shown in Figure 4. We use N_{ne}, N_{nw}, N_{sw} and N_{se} to indicate the number of extreme flares with source locations in the northeast, northwest, southwest and southeast quadrants of the solar disk respectively. As was shown in Figure 4, N_{ne}, N_{nw}, N_{sw} and N_{se} were 12, 14, 13 and 21, respectively. It was evident that the southeast quadrant had the largest number of extreme flares, indicating that the extreme flare activities in the southeast quadrant were the strongest compared with the three other quadrants during 1976–2018. It was found that 47.5% of the extreme flares occurred in the region with latitude $\leqslant 15°$, indicating that slightly less than half of the extreme flares appeared in the region with latitude $\leqslant 15°$ of both hemispheres. We also found that 42.6% of the extreme flares occurred in the

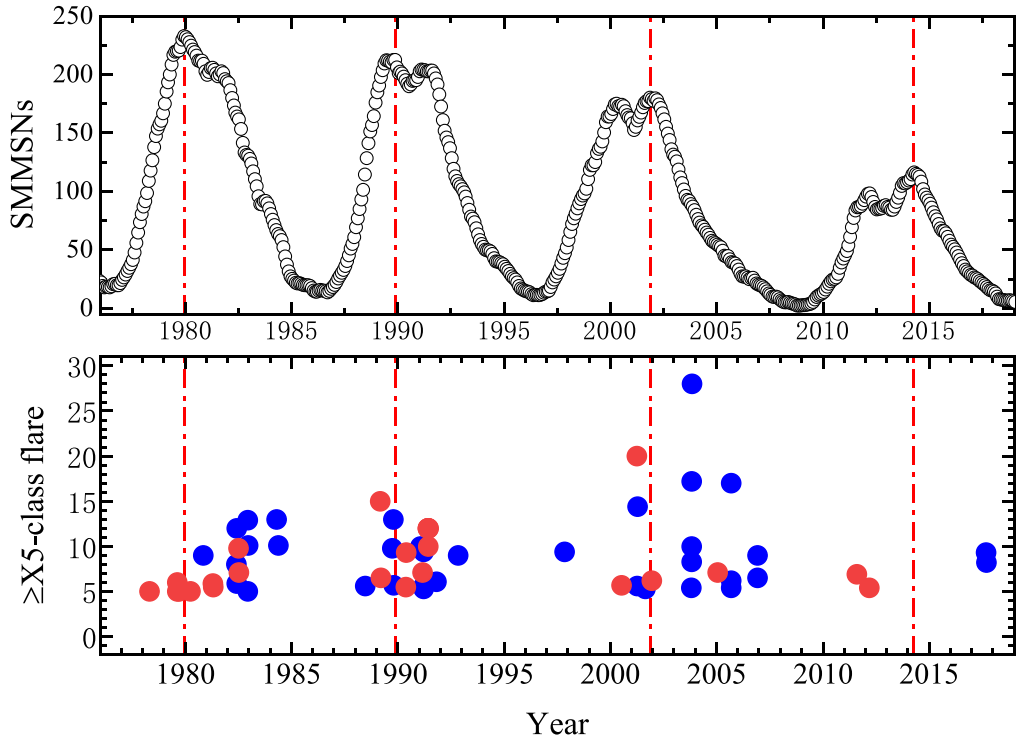

Figure 3. Solar cycle distribution of the extreme flares during 1976–2018. The red and blue solid circles indicate the flares with source locations in the northern and southern hemispheres, respectively.

latitudinal belt 11°–20° of the two hemispheres. Hence, the conclusion that the 11°–20° latitude belt of both hemispheres produced the most flares is not correct for the extreme flares during 1976–2018. We found that 31.1% of the extreme flares occurred in the region with latitude >20° of both hemispheres. 26.2% of the extreme flares occurred in the region with latitude ⩽10° of both hemispheres.

The N–S asymmetry of various solar activities has been the subject of extensive research (e.g., Deng et al. 2013; Deng et al. 2016, 2017, 2019; Javaraiah 2016; Chowdhury et al. 2019; Roy et al. 2020; Zhang et al. 2022; Zhao et al. 2022; Zhang et al. 2024). During the ascending phase of Solar Cycle 21, the N–S asymmetry was pronounced, with extreme flares occurring exclusively in the northern hemisphere. Applying the binomial formula as described by Larson (1982), the N–S asymmetry during the descending phase of Solar Cycle 21 was found to be insignificant. Nevertheless, the latitudinal distribution of extreme flares between the northern and southern hemispheres in this phase was asymmetric. The N–S asymmetry in the number of extreme flares during both the ascending and descending phases of Solar Cycle 22 was not significant; however, as depicted in Figure 1 and detailed in Table 1, the latitudinal distributions of extreme flares in both hemispheres were asymmetric. In the descending phase of Solar Cycle 23, extreme flares were predominantly observed in the southern hemisphere. During the ascending phase of Solar Cycle 24, extreme flares were more dominant in the northern hemisphere, while in the subsequent ascending phase, they were more prevalent in the southern hemisphere.

Figures 1 and 2 do not provide insights into the evolution of N–S asymmetry across solar cycles. For instance, during the descending phase of Solar Cycle 21, 14 extreme flares occurred, with nine originating from the southern hemisphere and five from the northern hemisphere, indicating a dominance of extreme flares in the southern hemisphere. However, as depicted in Figure 3, the northern hemisphere initially had more extreme flares than the southern hemisphere in the early part of the descending phase, with a gradual shift toward the southern hemisphere in the later part of the same phase (Oliver & Ballester 1994). They found that solar activity, as measured by sunspot areas, began to transition from the northern to the southern hemisphere during Solar Cycle 22. Joshi et al. (2006) observed that the northern hemisphere's dominance shifted toward the southern hemisphere after 2000 and persisted in subsequent years. Nevertheless, during the descending phase of Solar Cycle 22, the northern and southern hemispheres experienced eight and six extreme flares, respectively, suggesting a slight northern hemisphere excess. Joshi et al. (2015) noted that, generally, the northern hemisphere was more active during the ascending phases of cycles 21 to 23, while the

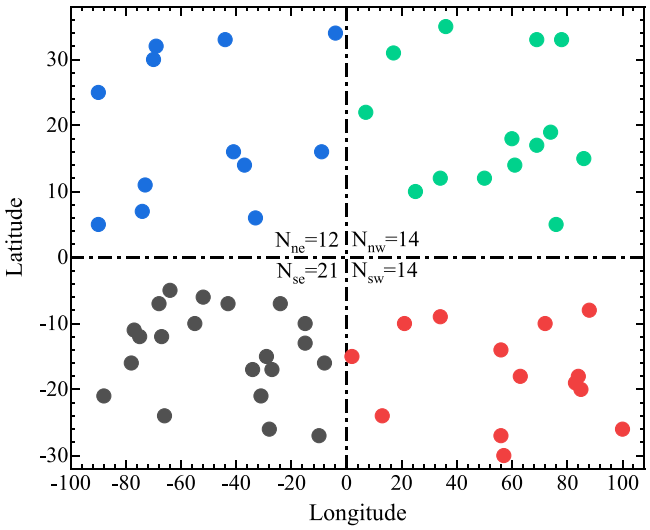

Figure 4. Source locations of the extreme flares during 1976–2018.

southern hemisphere took the lead during the descending phases. During the ascending phase of Solar Cycle 23, the northern and southern hemispheres had three and four extreme flares, respectively, indicating no clear dominance of extreme flares in the northern hemisphere. Overall, the N–S asymmetry exhibited by extreme flares differs somewhat from that shown by sunspot areas and flare indices during Solar Cycles 21–23.

If the extreme flares were split into two subgroups: the group1 (X5–X9) and the group2 ($\geqslant$X10), then group1 had 41 extreme flares, while group2 had 20 extreme flares. Of the 41 extreme flares in group1, 16 of them appeared in the ascending phases, i.e., 39% of the extreme flares of group1 appeared in the ascending phase. For the 20 extreme flares in group2, four extreme flares appeared in the ascending phases, i.e., 20% of the extreme flares of group2 appeared in the ascending phases. These indicate that the stronger the flares, the higher the proportion of the flares that occurred in the descending phase.

When extreme flares are categorized into two subgroups: Group 1 (X5–X9) and Group 2 ($\geqslant$X10). Group 1 contains 41 flares, and Group 2 contains 20 flares. Within Group 1, 16 flares, which is 39%, occurred during the ascending phases. In contrast, for Group 2, only four flares, or 20%, appeared during the ascending phases. This suggests that the more intense the flares, the greater the proportion that occurs during the descending phase.

4. Conclusions

Our study has focused on several aspects of extreme ($\geqslant$X5) solar flares from 1976 to 2018: the latitudinal distribution across individual solar cycles, the distribution of these flares in the four quadrants of the solar disk, the evolution of N–S asymmetry, and the solar cycle distribution of extreme flares. Based on these analyses, we can summarize our findings as follows:

(i) During Solar Cycle 21, a total of 18 extreme flares were recorded, with the majority occurring within the latitudinal belt of 5°–18° in both hemispheres. Solar Cycle 22 saw 21 extreme flares, of which 18 were distributed within the latitudinal belt of 20°–35° in both hemispheres. In Solar Cycle 23, 18 extreme flares occurred, with 16 of them concentrated within the latitudinal belt of 11°–22° in both hemispheres. Solar Cycle 24 had the fewest extreme flares, with only 4 recorded: two in the ascending phase at the same latitude of N17 from the northern hemisphere, and two in the descending phase at the same latitude of S08 from the southern hemisphere.

(ii) Among all extreme flares distributed across the four quadrants of the solar disk from 1976 to 2018, the southeast quadrant had the highest number of occurrences. The latitudinal distribution of these flares was as follows: 26.2% were within the range of 5°–10°, 31.1% were within the range of 11°–20°, and 42.6% were in regions with latitudes greater than 20°. Additionally, 47.5% of the extreme flares occurred in regions with latitudes less than or equal to 15°.

(iii) Extreme flares were predominantly observed during the ascending phase of Solar Cycle 21. In contrast, the N–S asymmetry during the descending phase of Solar Cycle 21 was primarily evident through the asymmetrical latitudinal distribution of extreme flares between the two hemispheres. Similarly, the N–S asymmetries in the extreme flares for both the ascending and descending phases of Solar Cycle 22 were reflected solely in the latitudinal distribution asymmetry. During the descending phase of Solar Cycle 23, extreme flares were largely concentrated in the southern hemisphere. In Solar Cycle 24, extreme flares showed dominance in the northern hemisphere during the ascending phase and in the southern hemisphere during the descending phase.

(iv) Extreme flares constituted 22.2%, 33.3%, 38.9%, and 50% of the activity during the ascending phases of Solar Cycles 21–24, respectively. This trend suggests that as the solar cycle strengthens, the proportion of extreme flares in the ascending phase decreases. Statistical analysis further reveals that 39% of flares classified as X1–X9 occurred during the ascending phases, compared to only 20% of flares with magnitudes $\geqslant$X10. This indicates that the stronger the flares, the more likely they are to occur during the descending phase of the solar cycle.

(v) A significant majority of extreme flares occurred in the period from two years before to three years after the solar maximum, with percentages of 88.9%, 100%, 61.1%, and 75% for Solar Cycles 21, 22, 23, and 24, respectively.

This variation suggests that the fraction of extreme flares appearing around solar maximum differs from one solar cycle to another. On average, 83.6% of extreme flares were observed within this period, highlighting the general tendency for extreme flares to peak around solar maximum.

Acknowledgments

The authors thank NOAA for providing the solar soft X-ray data and Solar Influences Data Analysis Center for providing smoothed monthly mean sunspot numbers at http://sidc.oma.be/silso/datafiles (accessed on 2024 June 1). This work was funded by the National Natural Science Foundation of China (NSFC) under Nos. 41074132, 41274193, 41474166, and 41774085, and the Special Fund of the Institute of Geophysics, China Earthquake Administration (Grant No. DQJB22X12).

Appendix
Extreme Flares During 1976–2018

The time information of year, month and day, and the source location of the latitude and longitude for each extreme flare during 1976–2018 are listed in Table A1.

Table A1
Extreme flares during 1976–2018

SC	No.	Year	Month	Day	Latitude	Longitude	Flare
21	1	1978	04	28	22	−41	X5
	2	1979	08	18	10	−90	X6
	3	1979	08	20	5	−76	X5
	4	1979	09	19	6	−33	X5
	5	1980	04	04	24	34	X5
	6	1980	11	06	−12	−74	X9
	7	1981	04	24	18	50	X5.9
	8	1981	04	27	15	86	X5.5
	9	1982	06	03	−9	−72	X8
	10	1982	06	04	−10	−55	X5.9
	11	1982	06	06	−9	−25	X12
	12	1982	07	09	17	−73	X9.8
	13	1982	07	12	11	−37	X7.1
	14	1982	12	15	−10	−15	X5
	15	1982	12	15	−10	−24	X12.9
	16	1982	12	17	−8	−21	X10.1
	17	1984	04	24	−12	−43	X13
	18	1984	05	20	−9	−52	X10.1
22	1	1988	06	24	−27	56	X5.6
	2	1989	03	06	35	−69	X15
	3	1989	03	17	33	60	X6.5
	4	1989	09	29	−18	84	X9.8
	5	1989	10	19	−10	−27	X13
	6	1989	10	24	−30	57	X5.7
	7	1990	05	21	35	36	X5.5
	8	1990	05	24	33	78	X9.3
	9	1991	01	25	−16	−78	X10
	10	1991	03	04	−24	−66	X7.1
	11	1991	03	07	−20	−66	X5.5
	12	1991	03	22	−26	−28	X9.4
	13	1991	03	25	−24	13	X5.3
	14	1991	06	01	25	−90	X12
	15	1991	06	04	30	−70	X12
	16	1991	06	06	33	−44	X12
	17	1991	06	09	34	−4	X10
	18	1991	06	11	31	17	X12
	19	1991	06	15	33	69	X12
	20	1991	10	27	−13	−15	X6.1
	21	1992	11	02	−26	−100	X9
23	1	1997	11	06	−18	63	X9.4
	2	2000	07	14	22	7	X5.7
	3	2001	04	02	19	74	X20
	4	2001	04	06	−21	−31	X5.6
	5	2001	04	15	−20	85	X14.4
	6	2001	08	25	−17	−34	X5.3
	7	2001	12	13	16	−9	X6.2
	8	2003	10	23	−21	−88	X5.4
	9	2003	10	28	−16	−8	X7.2
	10	2003	10	29	−15	2	X10
	11	2003	11	02	−14	56	X8.3
	12	2003	11	04	−19	83	X28
	13	2005	01	20	14	61	X7.1
	14	2005	09	07	−11	−77	X17
	15	2005	09	08	−12	−75	X5.4
	16	2005	09	09	−12	−67	X6.2
	17	2006	12	05	−12	−67	X6.2
	18	2006	12	06	−5	−64	X6.5
24	1	2011	08	09	17	69	X6.9
	2	2012	03	07	17	−27	X5.4
	3	2017	09	06	−8	33	X9.3
	4	2017	09	10	−8	88	X8.2

ORCID iDs

Qi Li https://orcid.org/0009-0005-5721-2906
Xi-Wen Zhang https://orcid.org/0009-0006-7914-1237
Gui-Ming Le https://orcid.org/0000-0002-9906-5132

References

Bai, T. 1987, ApJ, 314, 795
Bai, T. 1988, ApJ, 328, 860
Chapman, S. C., & Dudok de Wit, T. 2024, NatSR, 14, 8249
Chapman, S. C., Horne, R. B., & Watkins, N. W. 2020, GeoRL, 47, e2019GL086524
Chen, A., Wang, J., Li, J., Feynman, J., & Zhang, J. 2011, A&A, 534, A47
Chowdhury, P., Kilcik, A., Yurchyshyn, V., et al. 2019, SoPh, 2019, 142
Clette, F., & Lefèvre, L. 2016, SoPh, 291, 2629
Clette, F., Svalgaard, L., Vaquero, J. M., & Cliver, E. W. 2014, SSRv, 186, 35
Deng, L., Zhang, X., An, J., & Cai, Y. 2017, JSWSC, 7, A34
Deng, L. H., Qu, Z. Q., Liu, T., & Wang, K. R. 2013, AN, 334, 21
Deng, L. H., Xiang, Y. Y., Qu, Z. N., & An, J. M. 2016, AJ, 151, 70

Deng, L. H., Zhang, X. J., Li, G. Y., Deng, H., & Wang, F. 2019, MNRAS, 488, 111
Hajra, R., Tsurutani, B. T., Echer, E., Gonzalez, W. D., & Gjerloev, J. W. 2016, JGRA, 121, 7805
Javaraiah, J. 2016, AP&SS, 361, 208
Joshi, A., & Chandra, R. 2019, OAst, 28, 228
Joshi, B., Bhattacharyya, R., Pandey, K. K., Kushwaha, U., & Moon, Y.-J. 2015, A&A, 582, A4
Joshi, B., Pant, P., & Manoharan, P. K. 2006, JApA, 27, 151
Joshi, N. C., Bankott, N. S., & Pande, S. 2010, NewA, 15, 538
Kilpua, E. K. J., Olspert, N., Grigorievskiy, A., et al. 2015, ApJ, 806, 272
Larson, H. J. 1982, Introduction to Probability Theory and Statistical Inference (3rd ed.; New York: Wiley)
Le, G., Yang, X., Liu, Y., et al. 2014, Ap&SS, 350, 443
Le, G. M., & Liu, G. A. 2020, SoPh, 295, 35
Le, G. M., Liu, G. A., Zhao, M. X., Mao, T., & Xu, P. G. 2021a, RAA, 21, 130
Le, G. M., Zhang, Y. N., & Zhao, M. X. 2021b, SoPh, 296, 16
Le, G. M., Zhao, M. X., Li, Qi, et al. 2021c, MNRAS, 502, 2043
Le, G. M., Zhao, M. X., Zhang, W. T., & Liu, G. A. 2021d, SoPh, 296, 187
Lefèvre, L., Vennerstrøm, S., Dumbović, M., et al. 2016, SoPh, 291, 1483
Lin, J., Wang, F., Deng, L., et al. 2023, ApJ, 958, 1
Maunder, E. W. 1922, MNRAS, 82, 534
Meng, X., Tsurutani, B. T., & Mannucci, A. J. 2019, JGRA, 124, 3926
Oliver, R., & Ballester, J. L. 1994, SoPh, 152, 481
Owens, M. J., Lockwood, M., Barnard, L. A., et al. 2021, SoPh, 296, 82
Pandey, K. K., Yellaiah, G., & Hiremath, K. M. 2015, Ap&SS, 356, 215
Romano, P., & Zuccarello, F. 2007, A&A, 474, 633
Roy, J.-R. 1997, SoPh, 52, 53
Roy, S., Prasad, A., Ghosh, K., et al. 2020, SoPh, 295, 100
Tian, L. R., Liu, Y., & Wang, J. X. 2002, SoPh, 209, 361
Vennerstrom, S., Lefevre, L., Dumbović, M., et al. 2016, SoPh, 291, 1447
Verma, V. K. 2011, Ap&SS, 334, 83
Veronig, A., Temmer, M., Hanslmeier, A., et al. 2002, A&A, 382, 1070
Zhang, X., Deng, L., et al. 2024, ApJ, 962, 172
Zhang, X. J., Deng, L. H., Fei, Y., et al. 2022, MNRAS, 514, 1140
Zhao, M.-X., Le, G.-M., & Liu, Y.-H. 2022, Univ, 8, 605